Mon. Not. R. Astron. Soc. **000**, 000–000 (0000) Printed 21 September 2011 (MN LATEX style file v2.2)

New lensed quasars from the MUSCLES survey

Neal Jackson[1], Hayden Rampadarath[1,*], Eran O. Ofek[2,3], Masamune Oguri[4], Min-Su Shin[5]
[1] *Jodrell Bank Centre for Astrophysics, School of Physics & Astronomy, University of Manchester, Turing Building, Oxford Road, Manchester M13 9PL*
[2] *Division of Physics, Mathematics and Astronomy, California Institute of Technology, Pasadena, CA 91125, USA*
[3] *Einstein Fellow*
[4] *Institute for the Physics and Mathematics of the Universe, University of Tokyo, 5-1-5 Kashiwanoha, Kashiwa, Chiba 277-8583, Japan*
[5] *Department of Astronomy, University of Michigan, 500 Church Street, Ann Arbor, MI48109-1042, USA*

21 September 2011

ABSTRACT

Gravitational lens systems containing lensed quasars are important as cosmological probes, as diagnostics of structural properties of the lensing galaxies and as tools to study the quasars themselves. The largest lensed quasar sample is the SDSS Quasar Lens Search, drawn from the Sloan Digital Sky Survey (SDSS). We are attempting to extend this survey using observations of lens candidates selected from a combination of the quasar sample from the SDSS and the UKIRT Infrared Deep Sky Survey (UKIDSS). This adds somewhat higher image quality together with a wider range of wavelength for the selection process. In previous pilot surveys we observed 5 objects, finding 2 lenses; here we present further observations of 20 objects in which we find 4 lenses, of which 2 are independently discovered in SQLS (in preparation). Following earlier work on the combination of these two surveys, we have refined our method and find that use of a colour-separation diagnostic, where we select for separations between components which appear to decrease in wavelength, is an efficient method to find lensed quasars and may be useful in ongoing and future large-scale strong lensing surveys with instruments such as Pan-STARRS and LSST. The new lenses have mostly high flux ratios, with faint secondaries buried in the lensing galaxy and typically 6-10 times less bright than the primary. Our survey brings the total number of lenses discovered in the SDSS quasar sample to 46, plus 13 lenses already known. This is likely to be up to 60-70% of the total number of lensed quasars; we briefly discuss strategies by which the rest might be found.

Key words: gravitational lensing - cosmology:galaxy formation

1 INTRODUCTION

The first strong gravitational lens system was discovered over 30 years ago (Walsh, Carswell & Weymann 1979) and consisted of a quasar, lensed into two images about six arcseconds apart. Since then, over a hundred lensed quasars have been discovered by a variety of techniques.

Lensed quasars have a number of important uses. The most widely-studied application has been their use in determining the Hubble constant H_0 using measurements of time delays together with mass models for the lensing galaxy (Refsdal 1964); to date about 20 time delays have been measured (see e.g. Kochanek & Schechter 2004; Jackson 2007 for reviews). If H_0 is accurately known from other observations, the combination of a time delay and known cosmological world model allows the overall mass profile of the lens to be determined, independently of the mass sheet degeneracy (Gorenstein et al. 1988) which otherwise plagues such measurements. Lensed quasar light curves can also be used to study microlensing by stars in the lensed galaxy, (for a review see e.g. Wambsganss 1994); and variability as a function of wavelength in lensed quasars is a powerful tool for investigation of the structure of the quasars themselves. This approach has recently been used to constrain the sizes and structures of quasar accretion disks (Poindexter, Morgan & Kochanek 2008). Four-

* Current address: International Centre for Radio Astronomy Research, Curtin University, GPO Box U1987, Perth, WA 6845, Australia

image quasar lens systems are valuable as they can be used to study both dark and luminous substructures in the lensing galaxy (Mao & Schneider 1998, Dalal & Kochanek 2002, Kochanek & Dalal 2004, Vegetti et al. 2011, Jackson et al. 2010, Nierenberg et al. 2011). Finally, if statistically complete samples of quasar lenses can be compiled, their redshift and separation distributions are powerful probes of both cosmology and galaxy evolution (Ofek, Rix & Maoz 2003, Chae & Mao 2003, Oguri et al. 2008, Capelo & Natarajan 2007, Matsumoto & Futamase 2008).

Quasar lenses have hitherto been discovered in surveys of varying degrees of size and completeness. The largest of these surveys is the SDSS Quasar Lens Search (SQLS; Oguri et al. 2006, Oguri et al. 2008, Inada et al. 2010) in which a selection of quasars from the SDSS quasar list (Schneider et al. 2010) have been surveyed and 40 lens systems discovered to date[1] together with a further 2 so far in the survey described here. There are in total 105783 spectroscopically confirmed SDSS quasars in Data Release 7 (DR7), so a selection is made which targets apparently extended quasar images for observation as potential lenses. This is done either by morphological selection, for objects of separation less than $2\farcs5$ which are not deblended by the SDSS pipeline (York et al. 2000), or by colour selection for other objects. A variant of this method has been suggested by Kochanek et al. (2006) who proposed that all variable and extended objects in future surveys be targeted as potential lenses.

Unfortunately, it is difficult to make such surveys complete, as the initial finding survey throws up a number of false positives which must be eliminated. A significant source of contamination is chance alignment with the most common type of star, M stars. Because of the depth of both the SDSS and UKIRT Infrared Deep Sky Survey (UKIDSS), which contain quasars fainter than 19th magnitude, and the large size of the parent population of quasars, a significant number of M stars are expected within a typical Einstein radius of a number of SDSS quasars. Another source of contamination is foreground galaxies which are not close enough or massive enough to multiply image the background quasar, but which still require followup as they may contain a weak lensed image. These are significantly more difficult to eliminate from the search, as M stars have well-defined spectral features whereas many galaxies do not, and in the case of high-flux ratio lenses, the separation of a faint lensed image from the lensing galaxy can be difficult. This is especially the case because typical lensing geometries in two-image lens systems place the faint lensed image very close to the galaxy.

Several methods can be used to decrease the level of false positives. Firstly, we can use colour information to try and guess the nature of the secondary, and indeed SQLS uses colour cuts, particularly in the blue, to discriminate against systems where no quasar secondary is present – but at the cost of also discriminating against high flux-ratio lens systems. Secondly, high resolution is an important aid to lens-finding, because the median Einstein radius of a lens system is less than the typical ground-based seeing disk, corresponding to a typical lens galaxy which consists of an early-type system of 2-3L_* and $M \sim 10^{12} M_\odot$. In both of these respects it is helpful to use the UKIDSS survey (Lawrence et al. 2007) as an initial selection tool, because it expands the wavelength coverage into the infra-red and because its typical image quality ($0\farcs7$) is better than the typical image quality of SDSS ($1\farcs4$). The combined SDSS wavelength coverage, of 350-2200nm, covers a range in a typical lens system of a $z = 2$ quasar and $z = 0.5$ galaxy from the blue end, below the 4000Å break of the galaxy, where the quasar is expected to dominate the flux density and the red end, where the old stellar population of the lensing galaxy should dominate the flux. The MUSCLES (Major UKIDSS-SDSS Cosmic Lens Survey) has in the past used such a combination to discover two lenses: ULAS J234311.9-005034 (Jackson et al. 2008) and ULAS J082016.1+081216 (Jackson et al. 2009).

Here we extend the search with further observations. In section 2 we present our candidate selection and observations, and in section 3 we discuss the results. Finally we discuss, in section 4, the implications for future large surveys for quasar lenses.

2 CANDIDATE SELECTION AND OBSERVATIONS

2.1 Selection from SDSS and UKIDSS

Of the 105783 quasars from the SDSS DR7 (Schneider et al. 2010), 35356 are in the most recent footprint area of the UKIDSS, Data Release 8, and have images in at least one of the UKIDSS colours: Z, Y, J, H and K. UKIDSS uses the UKIRT Wide Field Camera (WFCAM; Casali et al, 2007); the photometric system is described in Hewett et al (2006), and the calibration is described in Hodgkin et al. (2009). The pipeline processing and science archive are described in Irwin et al (2011, in prep) and Hambly et al (2008). We ignore the Z band, as it has in general images of lower signal-to-noise than the other bands.

The UKIDSS images of all 35356 quasars were inspected by eye in order to find cases where the quasar image is extended. In principle, this can be done automatically using extension and ellipticity measurements for single objects in the UKIDSS database, together with selection of larger-separation lens candidates consisting of two UKIDSS objects close to each other. It is important to examine such cases individually, however, as automatic fitting is often unable to distinguish well between quasars residing in host galaxies, particularly at low redshift, and lens systems; automatically fitted ellipticity and extension parameters can then be used to check that nothing has been missed.

During the process which led to the discovery of ULAS J082016.1+081216, we identified an additional diagnostic, which arises due to the nature of quasar lens systems. If the quasar is lensed into a bright image A

[1] The current list is maintained at the SQLS website http://www-utap.phys.s.u-tokyo.ac.jp/~sdss/sqls/lens.html

and a normally weaker image B, the lens galaxy G lies along the line from A to B, but closer to B. In practice, G and B are unresolved by most ground-based optical images. However, because G is redder than B, the apparent separation between A and the G/B complex appears to decrease with increasing wavelength (Jackson et al. 2009; Rampadarath 2010). This effect is clearly seen in both the MUSCLES lenses, as well as a considerable number of SQLS lenses, and we use it here to help increase the efficiency of the survey.

Since the extensions in both SDSS and UKIDSS images are barely resolved, we measure the separation in a three-step process. First, we specify the positions of the two components approximately by eye, and fit for the fluxes only using two Gaussian profiles with a width approximately given by the PSF of the images. These fluxes are then used as initial inputs to a fit in which we allow the positions and fluxes of the centres of the two components to vary. Finally, we use the outputs of this iteration as inputs to another fitting iteration where all four parameters of each Gaussian (x- and y- position, flux, and width) are allowed to vary, subject only to the constraint that the two widths of the Gaussians should be equal[2]. This procedure was found to optimize the stability and uniformity of the fits, and to be robust in application to different images. Nevertheless, it does not always work well, usually for obvious reasons such as one of the images being extremely faint. The error on the separation is determined by the differences between the output positions in the second and third fitting iterations. This error is usually bigger than the photon statistics alone would indicate, but is more likely to be representative of the uncertainty in the fitting.

The search by eye alone yields a list of 947 candidates from the original sample of 35356. 213 objects were removed because of the available RA range during the observations, leaving 734; of these 348 were judged by eye to be of higher priority for observation. The Gaussian-fitting procedure was applied to this latter list.

2.2 WHT spectroscopic observations

Observations were made on the nights of 24 and 25 February 2011 using the ISIS double-arm spectrograph on the 4.2-m William Herschel Telescope on La Palma. All observations used a 300 lines mm^{-1} grating on the red arm, and a 158 lines mm^{-1} grating on the red arm. The slit width was changed to attempt to match the seeing, which varied from $0\farcs7$ to $2\farcs0$ during the observations, and the spectral resolution obtained therefore varies considerably from object to object. With the median slit of about $1''$ the spectral resolution was about 8 Å in the red arm and 4 Å in the blue. The plate scale was $0\farcs22\,\mathrm{pix}^{-1}$ in the red arm and $0\farcs20\,\mathrm{pix}^{-1}$ in the blue arm. For each object, a nearby offset star was used for acquisition, and in most cases a spectrum of the offset star was taken in order to measure the spatial profile of the system at a location close to the target. Relative flux calibration was achieved using the standard star SP0501+527 (Oke et al. 1995), and the wavelength scale was set using observations of Ne/Ar lamps once per night. All red-arm observations were centred on 730 nm, and blue-arm observations on 430 nm, allowing complete coverage of the visible spectrum from the atmospheric cutoff at 320 nm up to 900 nm, where the system sensitivity and night-sky lines cut off the useful spectral range. All objects were observed with a slit oriented along the position angle of the structure observed in the UKIDSS images.

Objects were selected for observation by eye, from the candidate list. Preference was given to objects which showed the separation-wavelength dependence outlined above, and in fact all such objects were observed. Objects at z>0.5 were also favoured, and objects at small separation were preferentially observed, as we know from radio lens searches such as CLASS (Myers et al. 2003, Browne et al. 2003), which are sensitive to all separations down to 300 mas, that these are more likely to be lens systems. Table 1 presents a complete summary of the observations; a total of 20 objects were observed. Fig. 1 shows the SDSS and UKIDSS images of the candidates.

The WHT data were reduced using a mixture of the NOAO IRAF package and other routines written in Python. Second-order polynomial solutions for wavelength against pixel number were derived from the arc exposures and applied to the data, straightening the spectral images in the wavelength direction in the process. The offset star exposures were used to derive a distortion correction which was then used to straighten each part of the object spectra into the same spatial pixel. Finally, the background was fitted and subtracted along the spatial direction in each column.

2.3 APO imaging observations

Two objects, 152720.1+014140 and 152938.9+103084, were observed with the SPIcam on the Astrophysical Research Consortium 3.5-meter telescope at the Apache Point Observatory on 2011 May 26. We binned the 2048^2 CCD by a factor of two along each axis during the readout, leading to a pixel scale of $0\farcs28$. The field of view is $4\farcm8$. For each object, we obtained three dithered exposures of 180 s in both g- and i-band under the seeing of $0\farcs9$. The images were reduced using standard IRAF tasks.

3 RESULTS

Inspection of the spectral images allowed immediate rejection of four candidates as potential lens systems, because the secondary was obviously an M star; these stars contain characteristic absorption bands at around 700 nm. This leaves 16 objects in which the secondary is likely to be a galaxy, either the host galaxy of the

[2] As these objects are potential lens systems, one object may be more extended than the other. However, our main purpose is to locate the distance between the centroids of two condensations, and the fixing of the width of each avoids giving too much freedom to the fit.

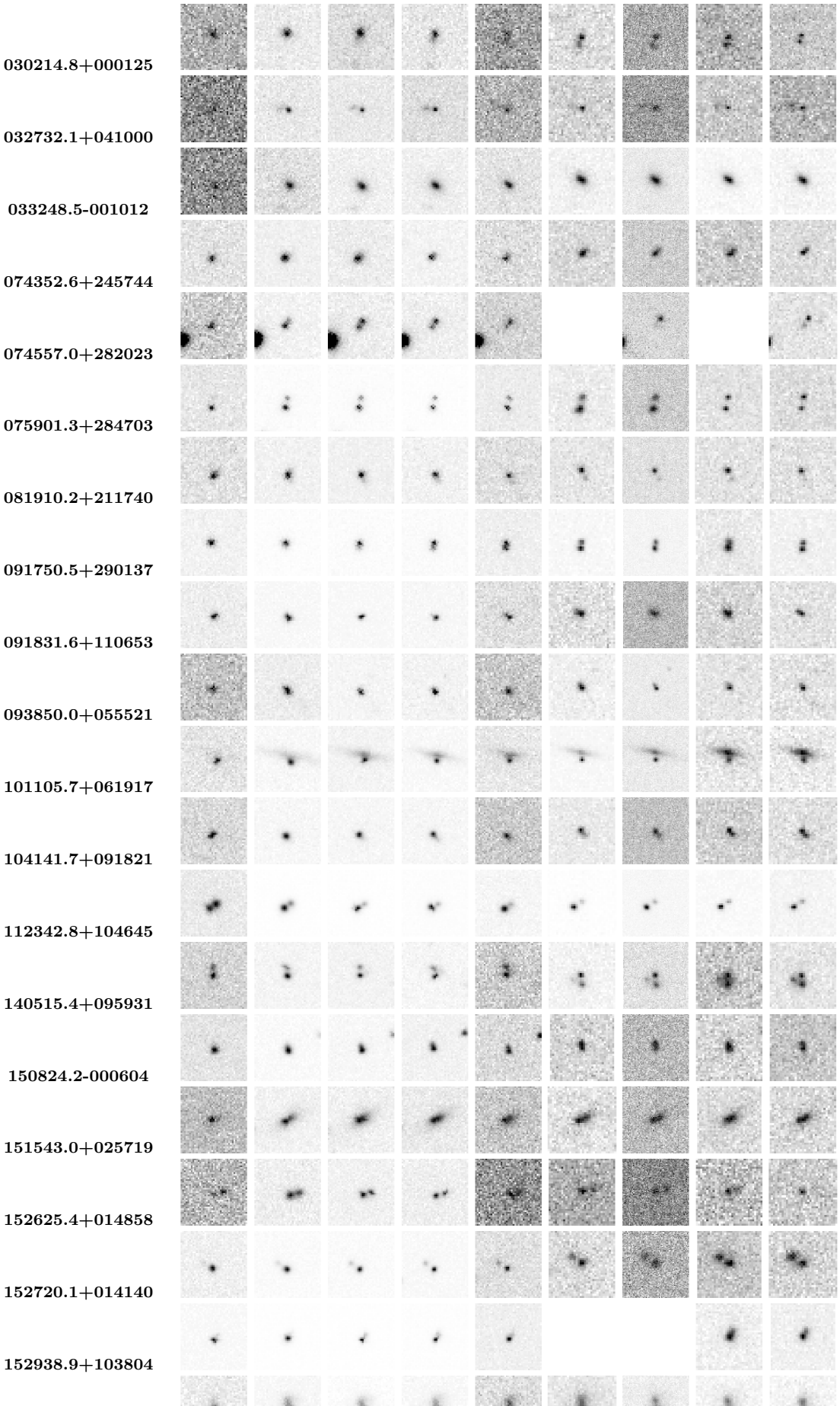
030214.8+000125
032732.1+041000
033248.5-001012
074352.6+245744
074557.0+282023
075901.3+284703
081910.2+211740
091750.5+290137
091831.6+110653
093850.0+055521
101105.7+061917
104141.7+091821
112342.8+104645
140515.4+095931
150824.2-000604
151543.0+025719
152625.4+014858
152720.1+014140
152938.9+103804

quasar, a lensing galaxy, or an association along the line of sight which is not close enough to lens the background quasar.

The diagnostic of a lens system is that the quasar emission lines are extended. In order to test this, we first fitted the spatial profile of a region of the spectral image which contains only the quasar continuum, using two Gaussians and using the width of the offset star's spatial profile to effectively measure the seeing and thus guide the fit to the quasar. This provided an accurate position on the chip, in the spatial direction, for the quasar and the nearby galaxy. Next, continuum regions around a quasar emission line were interpolated across the emission line and subtracted off each spatial row on the chip. This left only photons from the emission line. The emission-line region was then extracted in the spatial direction and fitted again, using the spatial positions of the quasar and galaxy which were previously determined in the continuum fit. A possible detection is considered to have been made if the flux within the secondary Gaussian is greater than five times the error on the fit.

We consider each gravitational lens, or possible gravitational lens, in turn. These are the objects in which the fitting procedure described produces evidence for the presence of extended emission lines. There are four objects with fairly certain identification as lens systems, and two where the identification is doubtful and requires further confirmation.

3.1 ULAS 074352.6+245743

ULAS 074352.6+245743 contains a z=2.167 quasar, and the UKIDSS images reveal a small separation (about 1.″0). The apparent separation between the fitted components is noticeably smaller in the infrared than in the optical, although some of the SDSS images are difficult to fit due to the object being barely resolved. The spectral fitting procedure has been applied to CIII], because CIV is of lower signal-to-noise and further into the blue where the seeing is worse, and MgII is badly contaminated by skylines. Fitting gives a 10σ detection of an extension to the line (Fig. 2) at a ratio of 6.4:1 between primary and secondary. The galaxy is detected at low signal-to-noise, and only at wavelengths of >550 nm. This suggests a redshift of a few tenths, although no absorption line is visible which might help to confirm this. This object has independently been identified as a likely lens by SQLS (unpublished; Oguri, private communication).

3.2 ULAS 140515.4+095931

This system, containing a quasar of redshift 1.810, was selected for observation because of a noticeable apparent decrease in separation with wavelength of its two components. It appears as a double system in most optical wavebands, but has an additional component to the east in the infrared. During the observations, the spectrograph slit was positioned N-S along the two brightest components. These are separated by 1.″95 (Fig. 3) with emission lines clearly present in both components. Spectra reveal an approximately 2:1 ratio in flux between the $z = 1.81$ quasar components, with very prominent associated absorption in both CIV and Lyα. The continuum colours of the two condensations are different, and consistent with the fainter quasar component being associated with a lensing galaxy. The lensing galaxy itself displays a likely 4000Å break, and possible emission lines at 655 and 660 nm; although these are of low signal-to-noise and require confirmation, this would imply an identification of CaH,K and a redshift of 0.66 for the lensing galaxy. Like ULAS 074352.6+245743, this object has independently been identified as a likely lens by SQLS (unpublished; Oguri, private communication).

3.3 ULAS 152720.1+014139

This is a clear example of a new lens system. It consists of two images of a z=1.439 quasar, separated by 2.″4. The spectrum around all of the major emission lines shows evidence of emission lines being clearly present in the secondary. The object moved along the slit between individual exposures in this object, but in all the exposures the two objects are seen with the same separation.

The spectrum (Fig. 4) shows the CIV, CIII] and MgII lines in both objects, with a flux ratio of 7.0±0.5:1. This is a relatively high ratio, similar to that obtained in many CLASS gravitational lenses. The two condensations in the optical and infrared images have very different colours, due to the weakness of the secondary lensed quasar image and consequent dominance of the lens galaxy over it at all but the bluest wavelengths. The different colours also immediately rule out the hypothesis that we are dealing with a binary quasar system as opposed to a gravitational lens. No absorption lines are present which might suggest the redshift of the galaxy, but the pronounced upturn in the spectrum between 500 and 600 nm is likely to be the 400 nm break feature of an early-type galaxy, leading to a probable redshift of about 0.3 for the lens galaxy. This system shows an apparent decrease in separation of the two components with wavelength; all of the UKIDSS images show a separation between the two components about 10% smaller than the SDSS optical images.

Fig. 4 also shows the APO i-band image of the system. This has been fitted using the GALFIT package (Peng et al. 2002) with two models; either two point sources, with PSFs determined from a nearby unsaturated star in the field, or two point sources plus a Sérsic profile to represent a possible lensing galaxy. The residuals from each fit show clearly that an extended object is required close to the secondary component, which we identify as the lensing galaxy (Table 2). The fit implies a flux ratio between the point sources of 9.7±0.9, slightly greater than that inferred from spectroscopy, and a separation of 2.″7±0.″1. The galaxy is fitted by a Sérsic profile of index 3.1 and effective radius of 0.″43, slightly elongated (b/a=0.66) in PA 13°. Because of the limited signal-to-noise, the fitted parameters of this galaxy are likely to be degenerate with each other, in particular the effective radius and Sérsic index.

Object	$z_{\rm SDSS}$	RA (J2000)	Dec (J2000)	Sep ($''$)	$T_{\rm exp}$(min)	slit PA	ID
030214.8+000125	1.179	03 02 14.823	+00 01 25.35	1.5	30	355	G
032732.1+041000	3.110	03 27 32.113	+04 10 00.09	2.1	45	80	G
033248.4−001012	0.310	03 32 48.497	−00 10 12.37	1.1	25	60	H
074352.6+245743	2.167	07 43 52.619	+24 57 43.64	1.2	40	135	L
074557.0+282023	1.558	07 45 57.015	+28 20 23.23	1.5(z)	45	141	G
075901.2+284703	2.849	07 59 01.287	+28 47 03.42	2.2	10	350	S
081910.1+211739	1.467	08 19 10.189	+21 17 39.54	1.6	45	200	G
091750.5+290137	1.816	09 17 50.529	+29 01 37.47	1.3	40	175	S
091831.5+110653	1.643	09 18 31.589	+11 06 53.05	1.2(z)	60	240	L?
093849.9+055520	1.983	09 38 49.991	+05 55 20.83	1.0	45	202	L?
101105.6+061917	1.946	10 11 05.672	+06 19 17.25	1.4	45	176	G
104141.7+091820	1.068	10 41 41.729	+09 18 20.55	1.6	75	40	G
112342.7+104645	1.635	11 23 42.769	+10 46 45.25	1.8	20	124	S
140515.4+095931	1.810	14 05 15.421	+09 59 31.30	1.8	45	0	L
150824.2−000603	1.578	15 08 24.221	−00 06 03.85	1.1	45	10	G
151543.0+025719	2.034	15 15 43.015	+02 57 19.35	1.5	55	300	H
152625.3+014857	2.987	15 26 25.389	+01 48 57.95	2.1	45	280	S
152720.1+014139	1.439	15 27 20.130	+01 41 39.60	2.4	75	60	L
152938.9+103803	1.971	15 29 38.902	+10 38 03.90	1.5	45	330	L
155104.1+261819	0.241	15 51 04.160	+26 18 26.00	1.8	15	5	H

Table 1. Objects observed in the programme. Coordinates and redshifts are from the SDSS. The final column (ID) represents the verdict of the analysis: S=quasar+star, H=quasar+host galaxy, G=quasar+probably unassociated galaxy, L=gravitational lens, L?=possible gravitational lens. Separations are measured using the UKIDSS Y-band images, except for two cases where this fit fails and the SDSS z-band is used instead.

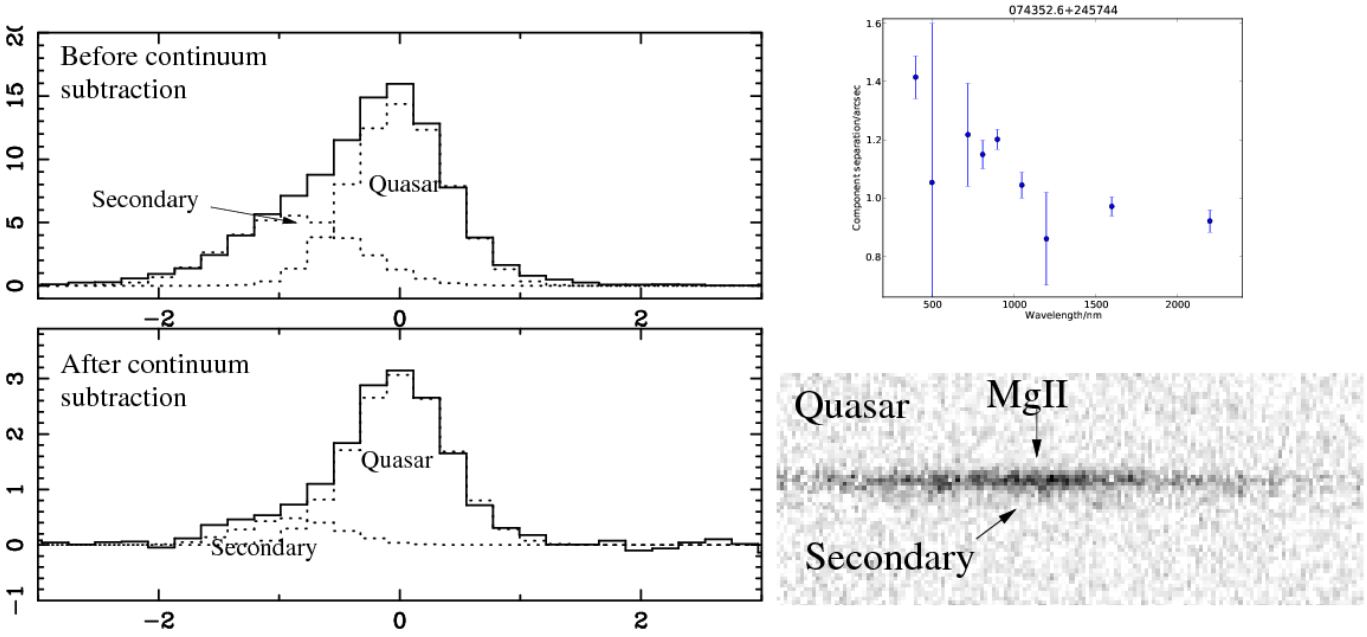

Figure 2. ULAS 074352.6+245743. Bottom right: part of the continuum-subtracted spectral image around MgII, showing a slight extension to the line. Top right: separation of the two components, as fitted to the SDSS (optical) and UKIDSS (infra-red) images, showing the apparently smaller separation in the infra-red due to the increased prominence of the lensing galaxy. Top left: fit to the spatial profile of the continuum around CIII], showing a clear extension due to either a companion galaxy or a lensing galaxy. Bottom left: spatial profile fit to the line part of the spectral image, now with the continuum subtracted row by row. Note that the raw profile is clearly asymmetric. A fit to the profile, with the same centroids as determined earlier, suggests an extended line of 16% of the flux of the primary line.

3.4 ULAS 152938.9+103803

This $z = 1.97$ quasar clearly has a secondary close to it. Fitting around the MgII line, as previously described, yields a secondary in the emission line with a flux ratio of 4.9±0.5 between the primary and secondary (Fig. 5) and a notional significance of 10σ. Fitting to the CIII] line, after subtraction, also shows an extended line, although here the continuum is more difficult to subtract. The blue frame also shows a likely extension to the CIV

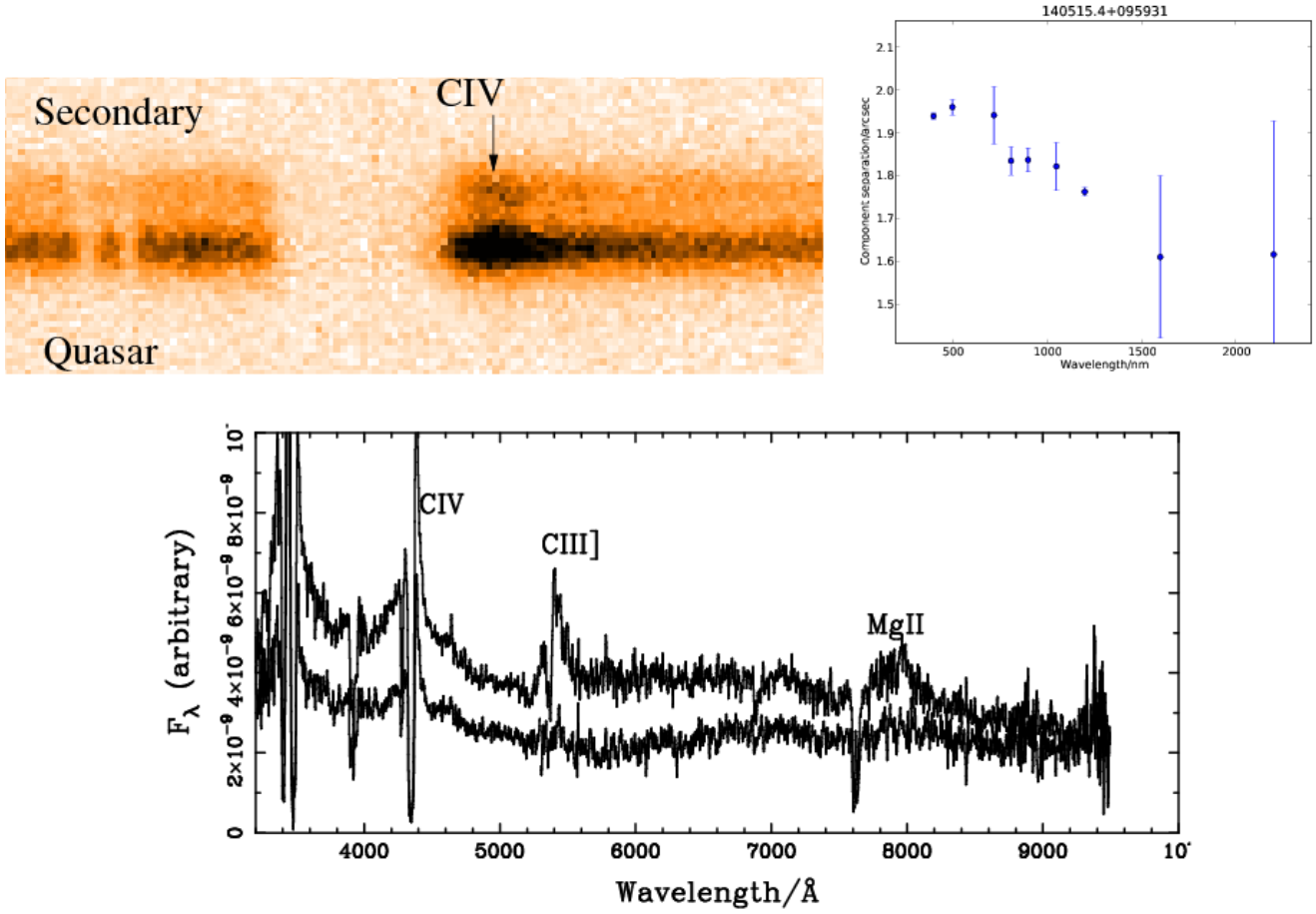

Figure 3. ULAS 140515.4+095931. Top left: part of the spectral image around MgII, showing the double line. Top right: separation of the two components, as fitted to the SDSS (optical) and UKIDSS (infra-red) images, showing the apparently smaller separation in the infra-red due to the increased prominence of the lensing galaxy. Bottom: WHT spectra, where the x-axis is observed-frame wavelength, of the primary and secondary objects. The lens is a 1.7:1 double. The A and B atmospheric bands have been blanked.

Object	Relative centroid	Relative flux	Sérsic index	Axis ratio (b/a)	r_e (arcsec)
152720.1-Q1	(0,0)	1.00	-	-	-
152720.1-Q2	(−2.20,1.38)	0.10	-	-	-
152720.1-G	(−1.86,1.24)	0.35	3.1	0.66	0.43
152938.9-Q1	(0,0)	1.00	-	-	-
152938.9-Q2	(0.69,1.18)	0.17	-	-	-
152938.9-G	(0.52,0.77)	0.17	2.0*	0.5*	0.30

Table 2. Parameters of GALFIT fits to the images of ULAS 152720.1+014139 and ULAS 152938.9+103803. Centroids in arcseconds (N,W) of the bright quasar image are given in column 2, and fluxes relative to the bright quasar image in column 3. A star indicates that this parameter has been fixed at a reasonable value in order to stabilise the otherwise badly constrained fit (see text). In the case of ULAS 152938.9+103803, the uncertainties on fluxes and positions of the weaker components are high (probably about 0.2 arcseconds in position). In both cases, Sérsic index and effective radius are degenerate.

line after continuum subtraction (Fig. 5). On the SDSS and UKIDSS images, there is a possible decrease in separation with wavelength, although the errors are high and some fits fail altogether due to the faintness of the secondary. The separation of the components on the spectra is 1.″2, although this is probably an underestimate because of the presence of the lensing galaxy; on the SDSS images we see a separation of about 1.″5.

These initial tests on the spectroscopic data are not conclusive, because the effects are relatively small in this object and may be subject to errors in the continuum fitting, as well as possible guiding errors. We therefore performed further tests, this time on the Lyα line in the blue spectrum. Each of the three independent spectral images from the three exposures with the ISIS blue arm was straightened so that the spectrum runs horizontally on the chip, and the continuum was again subtracted using a straight-line fit in each spatial pixel to areas blueward and redward of the line. For each frame, we then examined the spatial profile of

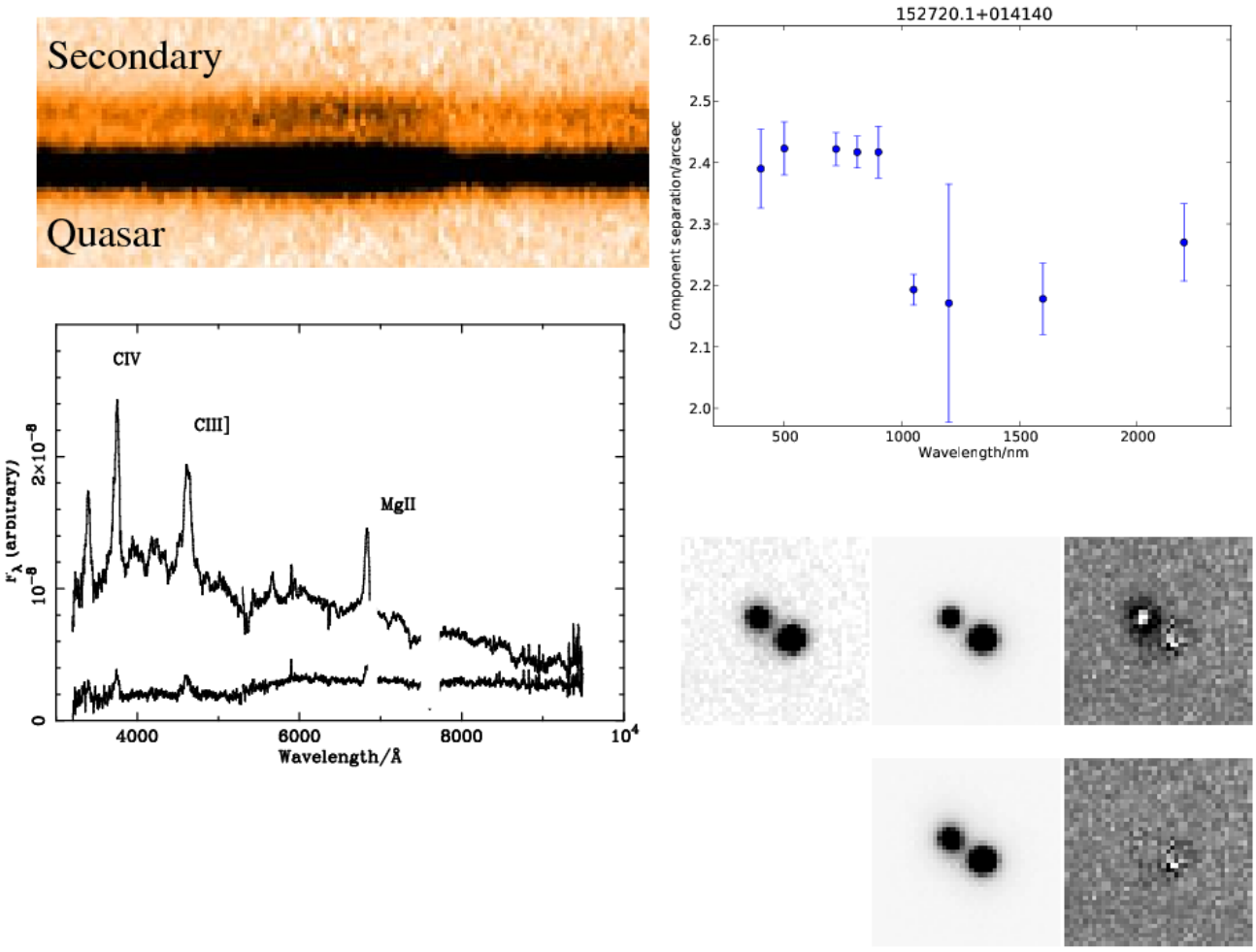

Figure 4. ULAS 152720.1+014139. Top left: part of the spectral image around MgII, showing the double line. Top right: separation of the two components, as fitted to the SDSS (optical) and UKIDSS (infra-red) images, showing the apparently smaller separation in the infra-red due to the increased prominence of the lensing galaxy. Bottom left: WHT spectra, where the x-axis is observed-frame wavelength, of the primary and secondary objects. The kinks in the spectrum at 5300 Åare the effects of the dichroic cut. The A and B atmospheric bands have been blanked. Bottom right: APO image (left) together with model and GALFIT residual with two point sources (top) and two point sources plus a Sérsic-profile galaxy (bottom).

the prominent absorption line in the centre of Lyα, together with the adjacent line emission (Fig. 5). Both the absorption line and emission line spatial profiles show asymmetry in the same direction, in all three frames. The fact that all three frames behave similarly suggests that telescope guiding errors are not the cause of the asymmetry in the spatial profiles. The fact that the asymmetry appears in the same direction in emission and absorption suggests that mis-subtraction of the continuum is not responsible, as an under-subtraction in the emission part of the line would correspond to an over-subtraction in the absorption part. This result should be robust for any type of mis-subtraction, including no subtraction of the continuum at all. We therefore conclude that the spectra provide evidence for an asymmetric profile of line emission, and hence the presence of a secondary image of the quasar.

The APO i-band images of this system (Fig.5) show the two main components clearly. Again, fitting using GALFIT to the image is difficult using only two PSFs. Inclusion of a Sérsic profile causes the χ^2 to fall by about 30% over the whole image, and a residual peak close to the fainter image to be removed. The fitting (Table 2) also implies a separation of about $1\farcs3$ between the two point components. However, the three-component fit is not well constrained due to the relatively low signal-to-noise; this free fit results in an extremely elliptical galaxy ($b/a = 0.06$) but good removal of the remaining residual. Constraining the galaxy to be more circular improves the residual by slightly less, but suggests a flux ratio of about 4–5 between the image components, close to that derived from spectroscopy. In both cases the effect of including a galaxy is to remove an extended region in the residual close to the weaker image.

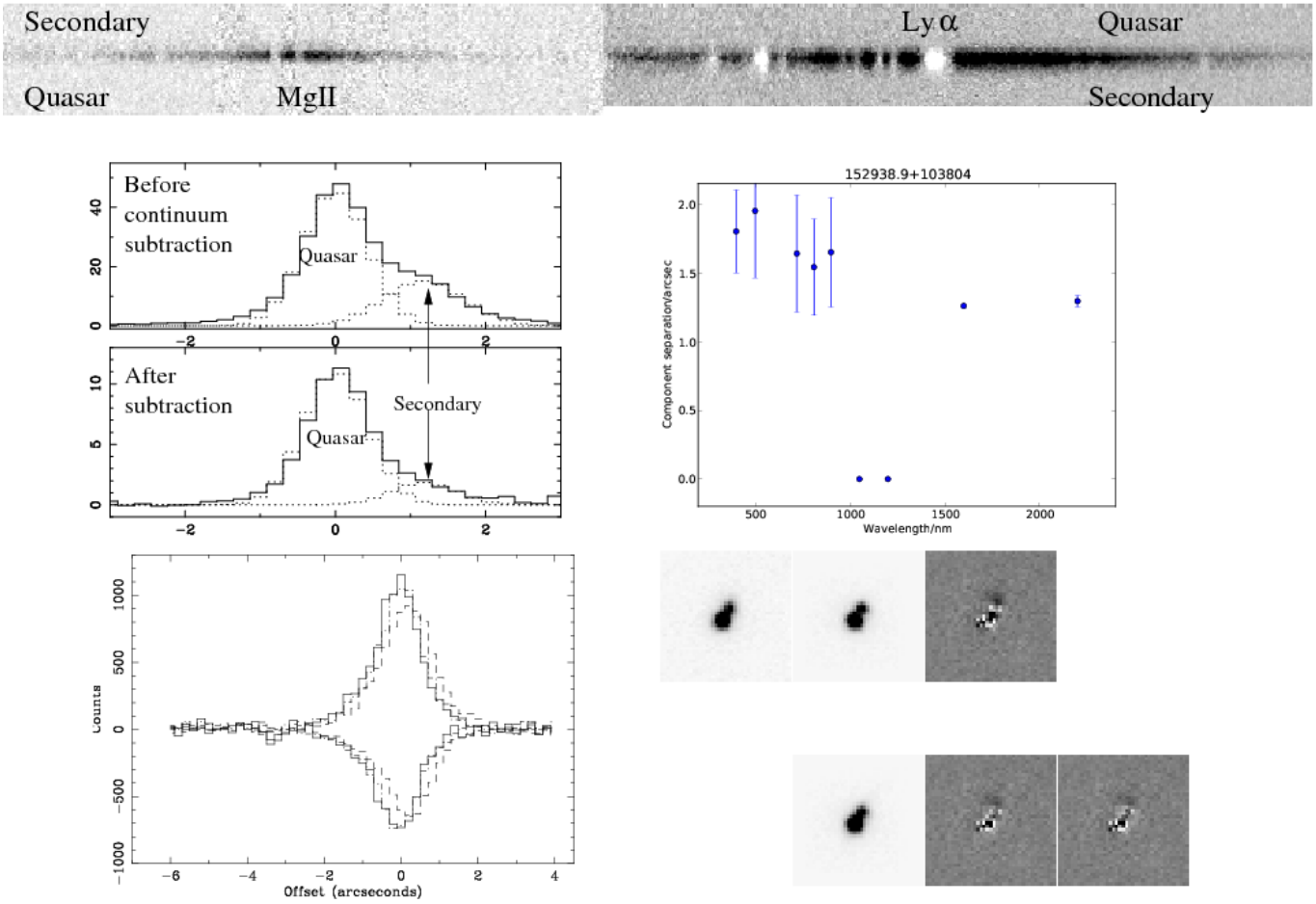

Figure 5. ULAS 152938.9+103803. Top: part of the continuum-subtracted spectral image around MgII(left) and Lyα (right), showing in each case a slight extension to the line. Middle left: separation of the two components in the spatial profile of the MgII line, at the top without subtraction of the continuum and at the bottom with continuum subtraction; a small residual remains, indicating the presence of extended line emission. The fit suggests extended line emission of about 17% of the primary. Middle right: fit to the separation of two components in the SDSS (optical) and UKIDSS (infra-red) images, showing the apparently smaller separation in the infra-red due to the increased prominence of the lensing galaxy. The fit fails in two cases just above 1000 nm. Bottom left: Spatial profile fits to the continuum subtracted Lyα emission line, from the three exposures separately (solid, dashed and dash-dotted lines), both for the prominent region of absorption and also for the adjacent emission region. All six profiles yield asymmetries, suggesting that the asymmetry observed is not due to mis-subtraction of the continuum or to guiding errors. Bottom right: APO image (left) together with model and GALFIT residual with two point sources (top) and two point sources plus a Sérsic-profile galaxy (bottom). In the second case, the residuals resulting from a free fit (left) and from a fit with b/a fixed at 0.5 and the Sérsic index fixed at 2.0 are shown.

3.5 ULAS 091831.5+110653 and ULAS 093849.9+055520

Two further objects still remain as candidates, although their status is uncertain. The first, ULAS 091831.5+110653, has a possible very slight extension on the SDSS images, in a direction just north of west. On the UKIDSS images the extension is more definite, and is likely to be much redder than the quasar itself. There is marginal evidence for an apparent decrease of separation with wavelength, although the z-image is probably the only SDSS image on which the extension appears with enough signal-to-noise for the separation to be determined with any accuracy. Fitting to the spectral image around the MgII line, with the continuum subtracted, gives a nominal 4σ detection of an extension to the line, but this is not very convincing given the uncertainties associated with the continuum subtraction and the Gaussian fitting to spatial profiles. The seeing was unfortunately not optimal during this observation, at about $1\farcs5$, and this object, while still a candidate lens system, requires further confirmation.

ULAS 093849.9+055520 is a candidate small-separation ($\sim 1\farcs0$) lens system. Unfortunately, the spectrum was taken during a period of poor seeing, the object has weak and broad emission lines, and the quasar redshift puts MgII in a bad region of OH skylines at around 830-840 nm. We attempted a fit of the line and continuum around CIV, but although it is possible to

derive an extended line profile, this is heavily dependent upon the fitting of each spatial row to subtract the surrounding continuum. This object, while still a candidate, therefore requires further observations to confirm or rule out its lensing status.

4 DISCUSSION AND CONCLUSIONS

Figure 6 shows an updated version of the relationship between separation and magnitude difference of SQLS and MUSCLES gravitational lens samples. The figure also includes a comparison with the CLASS sample, which is smaller but should be highly complete in both component flux ratio (<2.5 magnitudes) and separation. Since the CLASS survey was selected using VLA observations at 8.4 GHz, which have a diffraction-limited resolution of 0.″22, all lens systems on scales of 0.″3 should be detected, with some possibility of finding lenses on scales smaller than this.

About one-third of CLASS lenses have separations and flux ratios within the SQLS statistical sample limits (>1″and <1.25 mag, Inada et al. 2010). Within this range there are about 30 known lenses within the SDSS-DR7 quasars. Hence we expect about 90 lens systems in total from the SDSS-DR7 quasars, corresponding to a lensing rate of roughly 1:1000. The fact that 59 have been found to date (40 in SQLS, 13 previously known, 6 in the MUSCLES survey) suggest that only about 30 remain to be found. Those that remain are likely to be either of large flux ratio, leading to difficulties in separating the weak component from the lensing galaxy, or to be of small separation. Fig. 6 strongly suggests that a large majority of the lenses yet to be found in SDSS-DR7 are in the latter category. In principle, further research using the UKIDSS lens candidate systems can help to find the remaining objects, although the success rate is likely to drop. This is because the separation-wavelength diagnostic that we have developed is unlikely to be useful below about 1 arcsecond separation, as such systems will be completely unresolved on most SDSS images.

We have investigated the selection function of this survey in more detail using a simulation of the selection process. A large sample of simulated objects was generated for a range of primary-secondary flux ratios up to 2 magnitudes, and for a range of separations between 0 and 3 arcseconds. A magnitude for the primary object was chosen from the distribution of H-band magnitudes of SDSS quasars from the Schneider et al. (2010) catalogue, which is approximately described by a mean of 17.4 and a standard deviation of 0.78. For each simulated object, a random decision was taken by the algorithm on whether or not to include the secondary object, with equal probability of each outcome. A blind test was then undertaken for 2000 objects in which an observer (NJ) judged whether or not the quasar was extended, with the correct decision being scored as 1 and an incorrect decision as 0. Because half the simulated objects were lenses, by chance an average score of 0.5 would be expected, with 1.0 representing perfect discrimination in the selection process. In Fig. 7 we

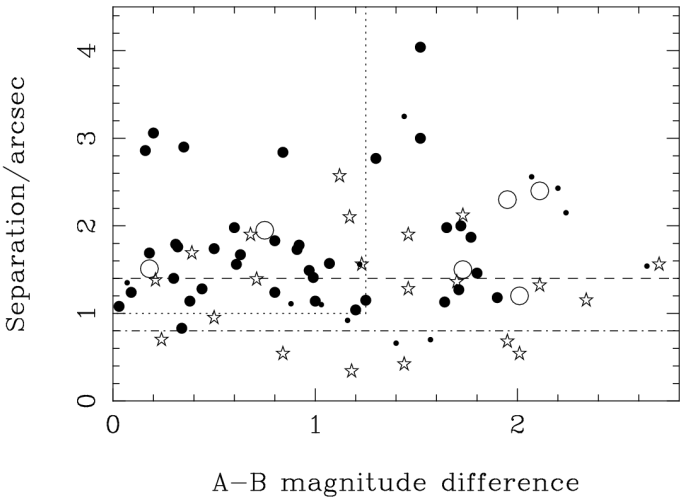

Figure 6. Updated plot of separation vs. magnitude difference between the brightest component and the next brightest component of gravitational lens systems (third brightest in the case of quad lenses). Large filled circles represent SQLS lenses, and small filled circles represent SDSS quasars already known before SQLS to be lens systems. Stars represent CLASS lens systems, which should be complete to a separation of 300 mas and a magnitude difference of 2.5. Open circles represent MUSCLES lenses from previous papers together with this work. The UKIDSS median image quality (dot-dashed line) and SDSS (dashed line) are indicated, together with the dynamic range and lens separation limit of the SDSS statistical sample (dotted line). Three SDSS lenses lie outside the plot due to large separation.

show the results of these simulations, binned according to flux ratio and separation. It is clear that the selection function involves both variables, with a very high probability of success for separations > 1″ and flux ratios less than one magnitude, but with significant probability of success at slightly smaller separations and higher flux ratios. The simulation was then repeated with 20000 objects, using the SEXTRACTOR package (Bertin & Arnouts 1996) for selection of extended objects. In this simulation, objects were deemed to be extended if more than one object was detected by SEXTRACTOR, or if a single object with major-to-minor axis ratio > r was fitted, with values of r of 1.3 and 1.5. The results are similar to those obtained by eye (Fig. 7). In principle, lower values of r give more efficient selection, although in practice, lowering r will increase vulnerability to false positives caused by effects not simulated here such as variable PSFs.

In fact, UKIDSS provides four images at different colours, which effectively increase the efficiency of selection of faint secondary images. To include this effect, the simulation was repeated with four images being generated for each field using different random noise. Fig. 7 (right panel) shows the results of this procedure, and it is now clear that >80% efficiency is achieved in selection for separation > 1″ and flux ratios <1.3 magnitudes, but with significant efficiency at or beyond 2.0 magnitudes. Unsurprisingly, the separation limit at just under 1″ is less affected by the extra information.

Looking at Figs. 6 and 7 together, it is probable that a few SDSS quasar lenses remain at high flux ratios, and

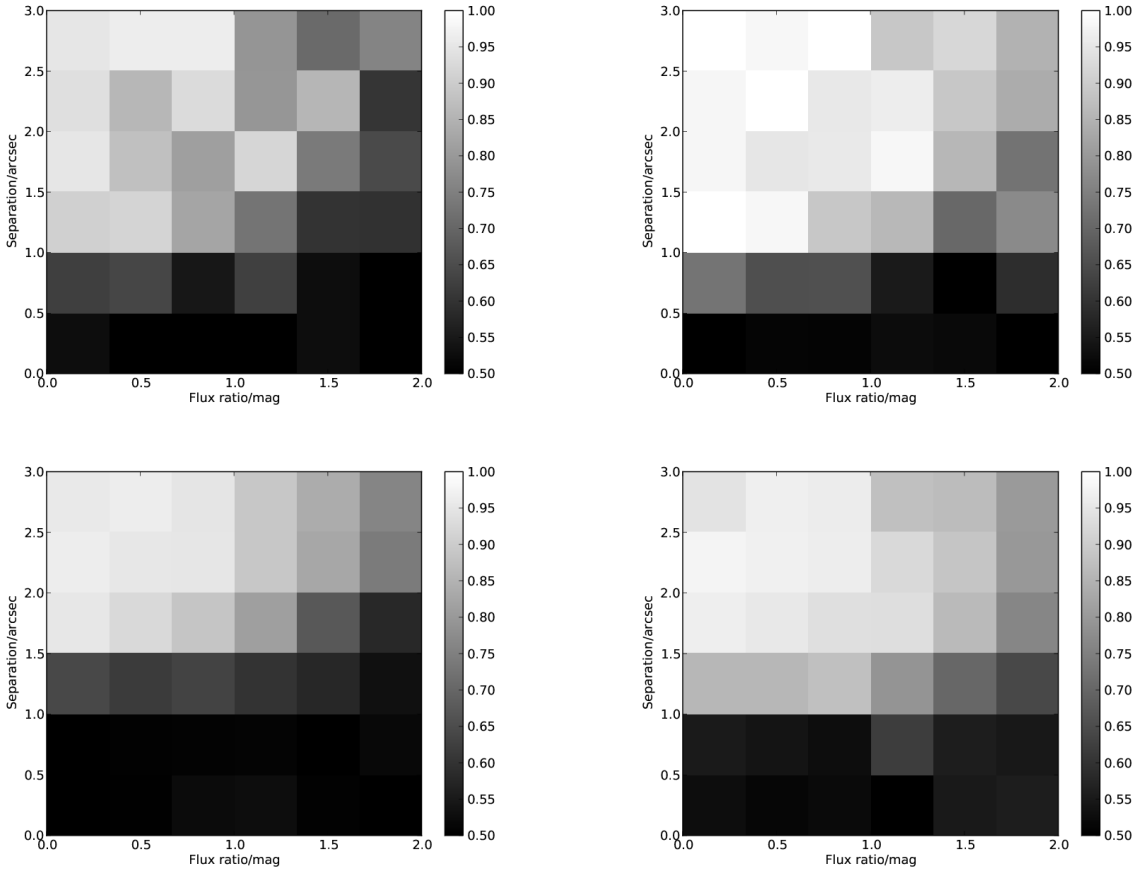

Figure 7. Fraction of correct results in simulations of lensed quasars as a function of separation and flux ratio, for a sample similar to UKIDSS (see text). A value of 0.5 is expected by chance, whereas perfect selection gives a value of 1.0. Top left: results obtained using one image and selection by eye. Top right: results obtained using four similar images, corresponding to the case for UKIDSS where images in four colours are available. Bottom: results obtained using one image and selection by SEXTRACTOR (see text) using r=1.5 (left) and r=1.3 (right).

that these lie in the half of the sky not yet fully covered by the MUSCLES programme. Such objects may well have been excluded from SQLS because of the colour criterion, with the secondary colour being dominated by the lensing galaxy. The majority (20-25 lenses) are likely to lie at separations less than 0.″8 - 0.″9, in the region where CLASS is much more efficient because of its three times higher resolution.

The results presented here have implications for quasar surveys using future generations of telescopes. In the near term, the Pan-STARRS survey (Kaiser et al. 2002), which is already operating, is expected to complete surveys of large areas of the sky with resolutions of about 1″; similar to, or a little better than, SDSS. Further into the future, the LSST project (Ivezic et al. 2008) expects to observe the entire southern hemisphere to much greater depth in multiple visits, with still better image quality (about 0.″7). This will find a very large number of strong lens systems (Oguri & Marshall 2010) but from a finding sample too large to rely on complete searches by eye, as has hitherto been possible (e.g. Jackson 2008) and automated algorithms will be required. In either case, isolation of complete samples of quasar lens systems in an automatic fashion based on imaging data alone is not a straightforward process, and is strongly dependent on image quality.

ACKNOWLEDGEMENTS

We thank Michael Strauss and Ian Browne for comments on the paper. The WHT is operated on the island of La Palma by the Isaac Newton Group of Telescopes at the Spanish Observatorio del Roque de los Muchachos of the Instituto de Astrofísica de Canarias. This work also uses data from the Apache Point Observatory 3.5-metre telescope, which is owned and operated by the Astrophysical Research Consortium. We would like to thank the Kavli Institute for Theoretical Physics and the organizers of the KITP workshop "Applications of Gravitational Lensing" for hospitality. This work began at this KITP workshop. HR was supported by the EU under the Marie Curie Early-Stage Training network MEST-CT-2005-19669 "Estrela". EOO is supported by an Einstein Fellowship and NASA grants. This work was supported in part by the National Science Foundation under grant

no. PHY05-51164 and by the Department of Energy contract DE-AC02-76SF00515. This work is based on data obtained as part of the UKIRT Infrared Deep Sky Survey, UKIDSS (www.ukidss.org). This work was supported in part by the FIRST program "Subaru Measurements of Images and Redshifts (SuMIRe)", World Premier International Research Center Initiative (WPI Initiative),MEXT, Japan, and Grant-in-Aid for Scientific Research from the JSPS (23740161). Funding for the SDSS and SDSS-II has been provided by the Alfred P. Sloan Foundation, the Participating Institutions, the National Science Foundation, the US Department of Energy, the National Aeronautics and Space Administration, the Japanese Monbukagakusho and the Max-Planck Society, and the Higher Education Funding Council for England. The SDSS web site is http://www.sdss.org/. The SDSS is managed by the Astrophysical Research Consortium (ARC) for the Participating Institutions.

REFERENCES

Bertin, E., Arnouts, S., 1996, A&AS, 117, 393
Browne I.W.A., et al., 2003, MNRAS, 341, 13.
Capelo P.R., Natarajan P. 2007, NewJPhys 9, 445
Casali M., et al., 2007, A&A, 467, 777.
Chae, K.-H., Mao, S., 2003, ApJ, 599, L61
Dalal, N., Kochanek, C.S., 2002, ApJ 572, 25
Gorenstein, M.V., Shapiro, I.I., Falco, E.E,, 1988, ApJ, 327, 693
Hambly N.C., et al. 2008, MNRAS, 384, 637.
Hewett P.C., Warren S.J., Leggett S.K., Hodgkin S.T. 2006, MNRAS, 367, 454.
Hodgkin S.T., Irwin M.J., Hewett P.C., Warren S.J., 2009,MNRAS, 394, 675
Inada N., et al., 2010, AJ, 140, 403.
Ivezic, Z., et al., 2008, Serbian Astron. J., 176, 1
Jackson N., 2008, MNRAS, 389, 1311
Jackson N., Ofek E.O., Oguri M. 2008, MNRAS, 387, 741.
Jackson N., Ofek E.O., Oguri M. 2009, MNRAS, 398, 1423
Jackson N., 2007, LRR, 10, 4
Jackson N., Bryan S., Mao S., Li C., 2010, MNRAS, 403, 826
Kaiser N., et al., 2002, SPIE, 4826, 154
Kochanek, C.S., Dalal, N., 2004, ApJ, 610, 69
Kochanek C.S., Schechter P., 2004, in "Measuring and Modeling the Universe", Carnegie Obs. Cent. Symp., ed. Freedman W.L., Cambridge University Press, p. 117
Kochanek, C.S., Mochejska,B., Morgan, N.D., Stanek, N.Z., 2006, ApJ, 637, L73
Lawrence A., et al., 2007, MNRAS, 379, 1599.
Mao, S., Schneider, P., 1998, MNRAS, 295, 587
Matsumoto A., Futamase T. 2008, MNRAS, 384, 843.
Myers S.T., et al., 2003, MNRAS, 341, 1.
Nierenberg, A., Auger, M.W., Treu, T., Marshall, P.J., Fassnacht, C.D., 2011, ApJ, 731, 44
Ofek E.O., Rix H.-W., Maoz D. 2003, MNRAS 343, 639
Oguri M., et al., 2006, AJ, 132, 999
Oguri, M., Marshall, P.J., 2010, MNRAS, 405, 2579
Oguri M., et al., 2008, AJ, 135, 512
Oke J.B., et al., 1995, PASP 107, 375
Peng C.Y., Ho L.C., Impey C.D., Rix H.-W., 2002, AJ 124, 266
Poindexter S., Morgan N., Kochanek C.S., 2008, ApJ, 673, 34
Rampadarath H., 2010, MSc thesis, University of Manchester
Refsdal S. 1964, MNRAS, 128, 307.
Schneider D.P., et al., 2010, AJ, 130, 2360
Vegetti S., Koopmans, L.V.E., Bolton, A.S., Treu, T., Gavazzi, R., 2011, MNRAS, 408, 1969
Wambsganss J., 1994, in Kochanek C.S., Schneider P., Wambsganss J., Proc. 33rd Saas-Fee Advanced Course, ed. Meylan G., et al., Springer-Verlag, Berlin
Walsh D., Carswell R., Weymann, R.J., 1979, Nature, 279, 381
York D.G., et al., 2000, AJ, 120, 1579